



Original Paper

Prediction of casing failure risk locations under multi-stage hydraulic fracturing inter-well interference in “well factory” mode



Yu-Heng Tuo, Tie-Jun Lin^{*}, Hao Yu, Zhang-Hua Lian, Fang-Xin Chen

State Key Laboratory of Oil and Gas Reservoir Geology and Exploitation, Southwest Petroleum University, Chengdu, 610000, Sichuan, China

ARTICLE INFO

Article history:

Received 6 September 2024

Received in revised form

21 February 2025

Accepted 23 February 2025

Available online 27 February 2025

Edited by Jia-Jia Fei

Keywords:

Well factory

Multistage fracturing

Fracture spatiotemporal evolution

In-situ stress redistribution

Casing failure prediction

ABSTRACT

The “well factory” mode’s high-density well placement and multi-stage hydraulic fracturing technology enable efficient development of unconventional oil and gas resources. However, the deployment of platform wells in the “well factory” model results in small wellbore spacing, and the stress disturbances caused by fracturing operations may affect neighboring wells, leading to inter-well interference phenomena that cause casing deformation. This study investigates the issue of inter-well interference causing casing deformation or even failure during multi-stage hydraulic fracturing in the “well factory” model, and predicts high-risk locations for casing failure. A flow-mechanics coupled geomechanical finite element model with retaining geological stratification characteristics was established. Based on the theory of hydraulic fracturing-induced rock fragmentation and fluid action leading to the degradation of rock mechanical properties, the model simulated the four-dimensional evolution of multi-well fracturing areas over time and space, calculating the disturbance in the regional stress field caused by fracturing operations. Subsequently, the stress distribution of multiple well casings at different time points was calculated to predict high-risk locations for casing failure. The research results show that the redistribution of the stress field in the fracturing area increases the stress on the casing. The overlapping fracturing zones between wells cause significant stress interference, greatly increasing the risk of deformation and failure. By analyzing the Mises stress distribution of multi-well casings, high-risk locations for casing failure can be identified. The conclusion is that the key to preventing casing failure in platform wells in the “well factory” model is to optimize the spatial distribution of fracturing zones between wells and reasonably arrange well spacing. The study provides new insights and methods for predicting casing failure in unconventional oil and gas reservoirs and offers references for optimizing drilling and fracturing designs.

© 2025 The Authors. Publishing services by Elsevier B.V. on behalf of KeAi Communications Co. Ltd. This is an open access article under the CC BY-NC-ND license (<http://creativecommons.org/licenses/by-nc-nd/4.0/>).

1. Introduction

The “Shale Revolution” has significantly boosted the oil and gas production capacity of the United States, mainstreaming the development of unconventional resources such as shale gas, shale oil, and tight sandstone gas. The development of these unconventional resources requires a large amount of drilling and fracturing operations. The traditional single-well operation mode is inefficient and costly, making it difficult to meet the demands of large-scale development. The development of horizontal well drilling technology and hydraulic fracturing technology has made the

extraction of unconventional oil and gas resources possible. These technologies necessitate centralized and standardized operational modes for efficient development. Some operators have adopted a production-oriented oil and gas field development strategy known as the “well factory” mode (Rexilius, 2015). The “well factory” operation mode is an oil and gas field development strategy that draws from manufacturing industry models. In limited well pad locations, a large number of laterals parallel to the reservoir are arranged. This approach minimizes surface land use while optimizing underground resource development, as illustrated in Fig. 1(a). These laterals usually use multi-stage hydraulic fracturing technology to modify unconventional reservoirs, increasing the modification rate within the regional reservoir to improve recovery rates, as shown in Fig. 1(b). Each section of the well is fractured independently to ensure maximum resource extraction (Liu et al.,

^{*} Corresponding author.

E-mail address: cwcttj@swpu.edu.cn (T.-J. Lin).

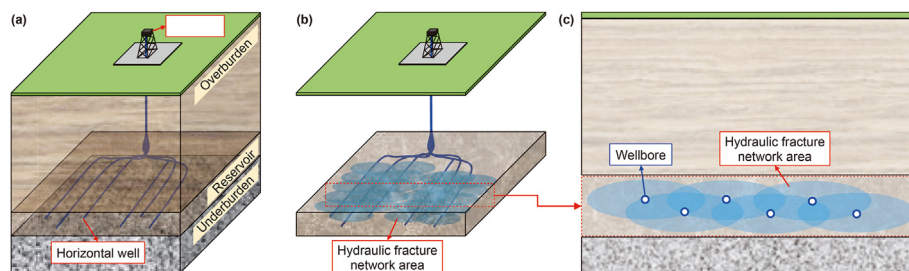


Fig. 1. Conceptual models of factory-style shale field development. (a) Block diagram of multiple benches with stacked laterals. (b) Multi-fractured parallel laterals. (c) Multi-fractured area cross section.

2017). By centralizing drilling, staged fracturing, and standardized operation processes, large-scale, low-cost, and high-efficiency oil and gas development can be achieved. Many oil and gas field companies worldwide have adopted the “well factory” model for developing unconventional oil and gas across large land areas, resulting in higher efficiency in drilling days and well costs. Data from several operators in the Eagle Ford Play in the United States shows that by using the well factory method, these operators reduced drilling costs and days by 40%, and reduced drilling days and well costs by up to 50%, significantly increasing EUR (Forbes et al., 2012; Huls et al., 2013; Nandlal and Weijermars, 2022). However, when operating in the “well factory” mode, as shown in Fig. 1(c), the simultaneous or sequential fracturing of two adjacent horizontal wells within a well pad can cause formation deformation and stress changes due to the injection of fracturing fluid and rock fracturing, forming a stress shadow. This stress shadow can affect the fracture propagation path and fracturing effectiveness of adjacent wells in the area to a certain extent, known as fracture interference between wells (Wang et al., 2015; Yu et al., 2017; Roussel and Sharma, 2011). Since 2020, more than 50% of horizontal wells in a certain continental shale oil production area in China have experienced well interference (Guo et al., 2021). Data from the Sulige Gas field in the Ordos Basin, China, shows that well interference is evident when the well spacing is less than 400 m, affecting production and wellhead pressure (He et al., 2012). Therefore, the significant problem of well interference in the “well factory” operational mode prompts the question of whether the stress shadow formed by fracturing will affect casing stress, leading to casing deformation and damage, warranting further investigation.

The problem of casing deformation and even failure after drilling and fracturing operations using the “well factory” model in unconventional reservoirs around the world has started to be frequently reported. Since fracturing is a necessary means of extracting unconventional resources, and to create high-speed channels for oil and gas to enter the wellbore in low-porosity, low-permeability reservoirs, large-scale volumetric fracturing is often used to modify such reservoirs. In the “well factory” operation mode, fracturing operations on one well have induced casing deformation and even failure in adjacent wells (Wang et al., 2024). Currently, some scholars believe that the casing deformation caused by volumetric fracturing in unconventional reservoirs is due to fluid entering and activating faults or natural fractures in the formation (Yu et al., 2023; Kostić et al., 2018; Lele et al., 2020; Jia et al., 2020). The sliding of these geological structures, after their original mechanical balance is disturbed, leads to the shearing deformation and failure of the casing passing through them (Tuo et al., 2024; Yin et al., 2018; Dong et al., 2019; Xi et al., 2021). They believe that the deformation of adjacent well casings is also caused by the slippage of activated faults. However, due to the need for large-scale volumetric fracturing in unconventional reservoirs,

the reservoir rock will be fractured by hydraulic forces, inevitably changing the mechanical properties of the regional rock mass and thus altering the stress field around the well. The in-situ stress around the well acts on the cement sheath outside the casing, which is the most direct and primary load on the outer wall of the casing. Changes in in-situ stress can directly lead to uneven loading on the casing, causing deformation and failure. This is why casing deformation problems remain significant in areas where faults or natural fractures are not developed. Lian, Li, and Lu, among others, studied the propagation patterns of fractures during multi-stage fracturing operations in conjunction with field geological conditions (Lian et al., 2015; Li et al., 2023; Lu et al., 2021). They used experiments or simulations to investigate the effects of formation stress state and hydraulic fracture propagation on the casing. Yu et al. believe that during the fracturing fluid pumping process, the stress field near the wellbore undergoes continuous redistribution and reorientation, resulting in some stress deficit and even tensile stress areas, putting the wellbore casing in this area in a “suspended” state (Yu et al., 2019, 2020). They observed that asymmetric fracturing areas generate strong shear stress on the suspended casing, leading to S-shaped deformation and an elliptical cross-section. Additionally, overlapping fracturing in certain areas exacerbates the heterogeneity of in-situ stress, further intensifying the severity of casing deformation. In the “well factory” operation mode, Kumar and Ghassemi established a three-dimensional model to simulate the propagation of multiple hydraulic fractures in multiple horizontal wells, calculating the propagation of multiple fractures during the continuous or simultaneous fracturing process of single and multiple horizontal wells, and analyzing various parameters affecting the interaction between dense fractures (Kumar and Ghassemi, 2016). Their research illustrates that in the “well factory” mode, the fracture network formed by fracturing a single well can extend into the formation area of adjacent wells to fully modify the reservoir. Hence, in the “well factory” operational mode, whether the fracturing modification areas of two horizontal wells will affect and interfere with each other concerning casing deformation and failure becomes a necessary direction for research on casing deformation and failure in unconventional reservoirs. Currently, this type of research is still lacking.

It is well known that the primary source of original in-situ stress in formations is the gravitational force on rock layers. The magnitude of vertical in-situ stress is basically equal to the pressure of the overlying rock layer, while horizontal in-situ stress mainly originates from the Poisson effect of rock deformation and geological structural differences. Therefore, it is necessary to understand the mechanical properties of rocks at different depths and the geological structural characteristics of the regional reservoir to calculate the distribution of the regional in-situ stress field. Additionally, in the “well factory” operation mode, multiple wells on the same platform require multi-stage hydraulic fracturing, and the

fracturing modification areas formed by different wells and fracturing stages differ in time and space. The fracture zones appear sequentially in the time domain with the fracturing order, and appear at different positions in the spatial domain. This causes the in-situ stress to continuously evolve in time and space as multi-well fracturing operations progress on the platform, thereby disturbing the external loads on the wellbore casing. In summary, to complete the study of in-situ stress changes and casing failure prediction under multi-well fracturing in the “well factory” operation mode, both geological and engineering factors must be considered.

In response to the above issues, this paper integrates rock mechanics, stress field redistribution, and the effects of multi-stage fracturing operations to provide a geological-engineering integrated computational model for predicting the failure risk locations of casings in platform horizontal wells under the “well factory” operation mode. The changes in rock mechanical properties after fracturing are calculated using the theory of mechanical strength degradation, taking into account fracture characteristics and fluid effects. Based on the characteristics of regional geological structures, a finite element model coupling seepage and geomechanics with multiple geological layers is constructed. Through multiple iterative matches with the interpreted data of in-situ stress logs from multiple exploratory wells in the region, the initial stress state of the reservoir is characterized. Utilizing image recognition and grid node coordinate identification technology, the four-dimensional distribution of the main fractures of two horizontal wells in time and space is depicted. The dynamic spatiotemporal evolution of the fracturing modification area and its disturbance to the regional in-situ stress field are simulated and calculated. By comprehensively considering the combined effects of multiple geological and engineering factors, the casing stress distribution under non-uniform in-situ stress is calculated. The risk of casing deformation and failure under multiple complex changes in the in-situ stress field around the well is predicted. Based on these findings, targeted optimization strategies are proposed. In summary, this paper offers new perspectives and methods for predicting casing failure risk through a comprehensive geological-engineering approach, stress field evolution simulation, multi-stage fracturing stress variation analysis, and the study of directional stress changes. This research has significant innovation and practical application value.

2. Mechanical effects of fracturing operations on casing

Under the “well factory” model, multi-well, multi-stage hydraulic fracturing operations can significantly increase the output of a single well, while maximizing the use of underground resources and reducing unit costs. This model centralizes the drilling and fracturing operations of multiple wells on a single platform, reducing the duplication of surface facilities, thereby improving economic efficiency and operational efficiency. However, in the pursuit of using hydraulic fracturing to form a complex fracture network in the reservoir and fully modify the reservoir, the mechanical strength of rocks in the fracturing modification area may degrade, leading to non-uniform redistribution of the in-situ stress field in the reservoir area. In a non-uniform stress field, the stress distribution on the casing will vary due to the complexity of formation conditions, impacting the integrity and safety of the wellbore.

2.1. Calculation of mechanical property degradation of rock in fracturing zone

After the rock in the fracturing transformation area is crushed, its mechanical properties degrade. Under the action of the original in-situ stress, the stress field around the wellbore will be disturbed and redistributed, increasing the non-uniformity of the external load on the casing and the risk of casing deformation failure.

The reservoir rock is considered a porous medium composed of a solid matrix and fully saturated micropores, as shown in Fig. 2(a). Therefore, fluid flow within the formation follows Darcy's law as follows:

$$\mathbf{v}_w = -\frac{1}{n_w g \rho_w} \mathbf{k} \cdot \left(\frac{\partial p_w}{\partial \mathbf{X}} - \rho_w \mathbf{g} \right) \quad (1)$$

where \mathbf{v}_w is the fluid velocity vector relative to the solid phase, m/s; n_w is the porosity, %; g is the gravitational acceleration vector, m/s²; ρ_w is the mass density of the fracturing fluid, kg/m³; \mathbf{k} is the permeability tensor, m/s. The fracturing fluid is assumed to be incompressible. The mass balance equation for a porous medium based on the principle of virtual work can be written as:

$$\int_V (\bar{\sigma} - p_w \mathbf{I}) \delta_\epsilon dV = \int_S \mathbf{f} \cdot \delta_\nu dS + \int_V \gamma \cdot \delta_\nu dV \quad (2)$$

The continuity equation for fluid flow within the formation can be expressed as:

$$\frac{1}{J} \frac{\partial}{\partial t} (J \rho_w n_w) + \frac{\partial}{\partial \mathbf{X}} \cdot (\rho_w n_w \mathbf{v}_w) = 0 \quad (3)$$

where \mathbf{X} is the spatial coordinate vector; $\bar{\sigma}$ is the effective stress tensor, MPa; p_w is the pore pressure, MPa; \mathbf{I} is the unit tensor (identity matrix) used to convert the scalar pressure p_w into an isotropic stress tensor, which represents the uniform fluid pressure exerted by the pore pressure in all directions. δ_ϵ is the virtual strain rate tensor; \mathbf{f} is the surface force vector, N; δ_ν is the virtual velocity vector, m/s; γ is the gravity vector, N; J is the formation volume change rate, which is the ratio of the formation volume in the current configuration to its volume in the original configuration, as shown in Fig. 2(b).

During each stage of fracturing, fracturing fluid is injected into the reservoir through perforations along the casing. According to fluid mass balance, a portion of the injected fluid during a certain period fills the enhanced production zone rich in fracture networks, while the remainder is lost into the surrounding matrix, as described by the following equation:

$$\frac{\partial V_f}{\partial t} + \nabla \cdot \mathbf{q} + (q_t + q_b) = q_{inj} \delta(x, y) \quad (4)$$

where V_f is the volume of the fracture, m³; q is the mass flow rate along each fracture, kg/s; q_t and q_b are the normal flow loss rates into the top and bottom layers of the reservoir, respectively; q_{inj} is the injection rate at known positions represented by the Dirac delta function $\delta(x, y)$, m/s, as shown in Fig. 2(c). Thus, the governing equations for the rock matrix include coupled fluid flow and rock deformation as follows:

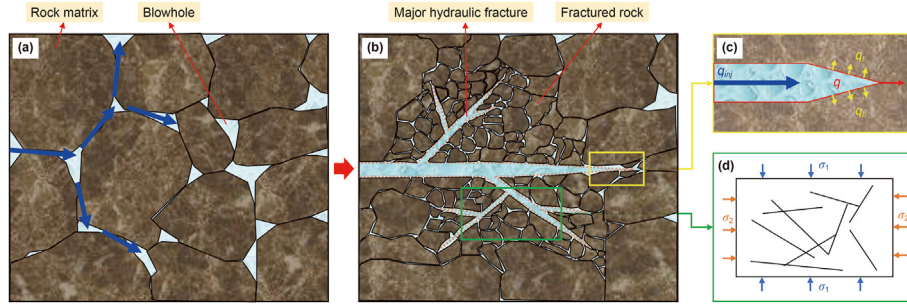


Fig. 2. Schematic diagram of the mechanism by which hydraulic fracturing operations cause local degradation of the mechanical properties of reservoir rocks. (a) Fluid flow in the porous medium before fracturing operations; (b) Fluid flow in the rock mass during fracturing operations; (c) Fluid flow and seepage loss in hydraulic fractures; (d) Stress diagram of the fractured rock mass.

$$\sigma_{ij} - \sigma_{ij}^0 = \frac{E}{1 + \nu} \left(\varepsilon_{ij} + \frac{\nu}{1 - 2\nu} \varepsilon_{kk} \delta_{ij} \right) - \alpha (p_w - p_w^0) \delta_{ij} \quad (5)$$

where σ_{ij} is the present in-situ stress component, MPa; σ_{ij}^0 is the original in-situ stress component, MPa; E is the Young's modulus of the rock matrix, MPa; ν is the Poisson ratio of the rock matrix; ε_{ij} is the strain component of the rock; ε_{kk} is the principal strain component; δ_{ij} is the Kronecker symbol, if $i \neq j$, $\delta_{ij} = 0$; If $i = j$, $\delta_{ij} = 1$; α is the Biot coefficient of the rock; and p_w^0 is the original pore pressure, MPa.

From a macroscopic perspective, hydraulic fracturing operations have a significant impact on the mechanical properties of rocks, including macroscopic elastic modulus and Poisson's ratio. As illustrated in Fig. 2(d), hydraulic fracturing breaks the rock, generating numerous fractures and broken zones, leading to a decrease in the overall stiffness of the rock mass. Therefore, the macroscopic elastic modulus generally decreases. The presence of fractures makes the rock more prone to deformation under external forces, thereby reducing its elastic modulus. The extent of reduction in the macroscopic elastic modulus of the rock mass is influenced by various factors, such as the number, width, and distribution of fractures, the initial mechanical properties of the shale, the nature of the fracturing fluid, and the injection pressure, making it difficult to accurately determine the change pattern through theoretical calculations. Different studies and practical cases indicate that the change in elastic modulus ranges roughly between 10% and 50%. The change in Poisson's ratio is more complex, depending on factors such as the shape and distribution of fractures and the extent of fracture healing after fracturing. Generally, an increase in fractures within the rock will affect its lateral deformation characteristics, causing Poisson's ratio to either increase or decrease. If the fractures cause more significant lateral deformation of the rock under compression, Poisson's ratio may increase. If the fractures are numerous and wide, lateral deformation is restricted, and Poisson's ratio may decrease. The change in Poisson's ratio is complex, and the specific range of change is difficult to determine uniformly, but it generally ranges between 5% and 20% (Warpinski et al., 2009).

To summarize this section, the mechanical properties of reservoir rocks in the hydraulic fracture network area are affected by the coupling of fluid mechanics and fracture solid mechanics. In real formations, the spatial distribution of hydraulic fractures is highly random and uncertain. Obtaining accurate mechanical properties and stress states at various locations in three-dimensional space on a macroscopic scale involves a significant computational cost when analytically calculating the impact of fracturing operations on the reservoir rock mass. Therefore, this paper, based on the calculation of the stress field in the reservoir area using a seepage-mechanics coupled geomechanical model, depicts the main fractures in

hydraulic fracturing within the model. It controls the changes in formation fluid pressure and rock mechanical parameters during the fracturing process using a user-defined field, thereby simulating the disturbance of the regional stress field induced by hydraulic fracturing operations.

2.2. Stress distribution inside casing in non-uniform stress fields

After hydraulic fracturing, the mechanical properties of the reservoir rock mass deteriorate, and the regional stress field is redistributed, greatly increasing the likelihood of enhanced non-uniformity in the stress around the wellbore, thereby increasing the risk of casing deformation and failure due to non-uniform external loads. Therefore, to predict the possible locations of casing failure, it is necessary to calculate the stress distribution on the casing.

Let the outer radius and inner radius of the casing be a and a_0 , m, respectively. The maximum principal stress and minimum principal stress of the original in-situ stress are denoted as σ_H and σ_h , MPa, respectively. The internal pressure of the casing is p_0 , MPa. Using the convention of elasticity, tensile stress is positive and compressive stress is negative, with the maximum principal stress direction taken as the x -axis direction. Introduce the mean stress σ and deviatoric stress s , represented as:

$$\begin{aligned} \sigma &= (\sigma_H + \sigma_h)/2 \\ s &= (\sigma_H - \sigma_h)/2 \end{aligned} \quad (6)$$

Therefore, the boundary conditions at the outer edge, specifically on the circumference ($r = b$) far beyond the outer radius a of the casing within the formation, for the radial normal stress and tangential shear stress can be expressed as:

$$\sigma_r(b) = -\sigma - s \cos 2\theta \quad (7)$$

$$\tau_{r\theta}(b) = s \sin 2\theta \quad (8)$$

The inner boundary conditions are:

$$r = a_0, \sigma_r(a_0) = -p_0, \tau_{r\theta}(a_0) = 0 \quad (9)$$

The original problem can be decomposed into two sub-problems, each with their respective boundary conditions:

$$r = b, \sigma_r(b) = -\sigma, \tau_{r\theta}(b) = 0 \quad (10)$$

$$r = a_0, \sigma_r(a_0) = -p_0, \tau_{r\theta}(a_0) = 0 \quad (11)$$

And,

$$r = b, \sigma_r(b) = -s \cos 2\theta, \tau_{r\theta}(b) = s \sin 2\theta \tag{12}$$

$$r = a_0, \sigma_r(a_0) = 0, \tau_{r\theta}(a_0) = 0 \tag{13}$$

Solving for the casing load under boundary conditions (10) and (11) constitutes an axisymmetric problem, referred to as Problem A; solving under boundary conditions (12) and (13) constitutes Problem B. After obtaining solutions for these two problems, their superposition yields the solution to the original problem.

Let E_s and ν_s denote the elastic modulus and Poisson's ratio of the formation, and E_c and ν_c denote the elastic modulus and Poisson's ratio of the casing, respectively. Let $m = a_0/a$ represent the ratio of the inner to outer radius of the casing. According to the fundamental solution of the Lamé problem for displacement, we have:

$$u_r(r) = \frac{(1 + \nu)r}{E(b^2 - a^2)} \left[(1 - 2\nu)(a^2q_1 + b^2q_2) + \frac{a^2b^2}{r^2}(q_1 + q_2) \right] \tag{14}$$

$$\begin{cases} \sigma_r^c(r) = \frac{a_0^2}{a^2 - a_0^2} \left(1 - \frac{a^2}{r^2}\right) p_0 + \frac{a^2}{a^2 - a_0^2} \left(1 - \frac{a_0^2}{r^2}\right) s_1 - \left[n_1 + n_2 \left(\frac{a}{r}\right)^4 + 2n_4 \left(\frac{a}{r}\right)^2 \right] \cos 2\theta \\ \sigma_\theta^c(r) = \frac{a_0^2}{a^2 - a_0^2} \left(1 + \frac{a^2}{r^2}\right) p_0 + \frac{a^2}{a^2 - a_0^2} \left(1 + \frac{a_0^2}{r^2}\right) s_1 + \left[n_1 + n_2 \left(\frac{a}{r}\right)^4 + 2n_3 \left(\frac{a}{r}\right)^2 \right] \cos 2\theta \\ \tau_{r\theta}^c(r) = \left[n_1 - n_2 \left(\frac{a}{r}\right)^4 + n_3 \left(\frac{a}{r}\right)^2 - n_4 \left(\frac{a}{r}\right)^2 \right] \sin 2\theta \end{cases} \tag{20}$$

where a and b are the inner and outer radii of the thick-walled cylinder, m ; q_1 and q_2 represent the internal pressure and external tension applied to the thick-walled cylinder, MPa. For the formation region, at $r = a$, the displacement of Problem A in the formation is

$$u_r(r) = \frac{(1 + \nu)r}{E(b^2 - a^2)} \left[(1 - 2\nu)(a^2q_1 + b^2q_2) + \frac{a^2b^2}{r^2}(q_1 + q_2) \right] \tag{15}$$

Here, s_1 represents the algebraic value of the surface load on the casing to be determined. Applying Eq. (11) to the casing region (with outer radius a and inner radius a_0), we have:

$$\begin{aligned} \sigma_r(a_0) &= -q_1 = -p_0 \\ \sigma_r(a) &= q_2 = s_1 \end{aligned} \tag{16}$$

Setting $r = a$, the displacement of the casing at $r = a$ is:

$$u_r^{Ac}(a) = \frac{(1 + \nu_c)a}{(1 - m^2)E_c} \left[(1 - 2\nu_c + m^2)s_1 + 2(1 - \nu_c)m^2p_0 \right] \tag{17}$$

Considering the continuity of displacement at $r=a$ between the formation and the casing, $u_r^{As}(a) = u_r^{Ac}(a)$, $u_r^{As}(a)$ is the radial displacement of the formation, $u_r^{Ac}(a)$ is the radial displacement of casing. So the casing load is obtained as:

$$s_1 = -2 \left[(1 - 2\nu_s)\sigma + \frac{1 - \nu_c^2}{1 + \nu_s} \frac{E_s}{E_c} \frac{m^2}{1 - m^2} p_0 \right] \left[1 + \frac{1}{1 - m^2} \frac{1 + \nu_c}{1 + \nu_s} \frac{E_s}{E_c} (1 - 2\nu_c + m^2) \right]^{-1} \tag{18}$$

Taking $q_1 = p_0$ and $q_2 = s_1$, the stress in casing for Problem A is:

$$\begin{cases} \sigma_r^{Ac}(r) = \frac{a_0^2}{a^2 - a_0^2} \left(1 - \frac{a^2}{r^2}\right) p_0 + \frac{a^2}{a^2 - a_0^2} \left(1 - \frac{a_0^2}{r^2}\right) s_1 \\ \sigma_\theta^{Ac}(r) = \frac{a_0^2}{a^2 - a_0^2} \left(1 + \frac{a^2}{r^2}\right) p_0 + \frac{a^2}{a^2 - a_0^2} \left(1 + \frac{a_0^2}{r^2}\right) s_1 \\ \tau_\theta^{Ac}(r) = 0 \end{cases} \tag{19}$$

Combining the solutions from Problem B, the stress distribution inside the casing in a non-uniform stress field considering internal pressure is:

where,

$$\begin{cases} n_1 = -\frac{1}{2}(s_2 - s_3) \frac{1 + m^2 + 4m^4}{(1 - m^2)^3} - \frac{1}{2}(s_2 + s_3) \frac{1 + m^2}{(1 - m^2)^3} \\ n_2 = -\frac{3}{2}(s_2 - s_3) \frac{m^4(1 + m^2)}{(1 - m^2)^3} - \frac{1}{2}(s_2 + s_3) \frac{m^4(3 - m^2)}{(1 - m^2)^3} \\ n_3 = 3(s_2 - s_3) \frac{m^2}{(1 - m^2)^3} + (s_2 + s_3) \frac{1}{(1 - m^2)^3} \\ n_4 = (s_2 - s_3) \frac{m^2(1 + m^2 + m^4)}{(1 - m^2)^3} + (s_2 + s_3) \frac{m^2}{(1 - m^2)^3} \end{cases} \tag{21}$$

in Eq. (21), the casing load parameters s_2 and s_3 are:

$$\begin{aligned} s_2 &= \frac{C_{22} + C_{12}}{C_{11}C_{22} - C_{12}C_{21}} R \\ s_3 &= -\frac{C_{21} + C_{11}}{C_{11}C_{22} - C_{12}C_{21}} R \end{aligned} \tag{22}$$

where,

$$\begin{cases}
 C_{11} = \left(1 - \frac{2}{3}v_c\right) + (5 - 6v_c)m^2 + (3 - 2v_c)m^4 + \left(\frac{5}{3} - 2v_c\right)m^6 + \frac{1 + v_s}{1 + v_c} \frac{E_c}{E_s} \left(\frac{5}{3} - v_s\right) (1 - m^2)^3 \\
 C_{12} = C_{21} = -\frac{2}{3}v_c + 2v_cm^2 - 2(2 - v_c)m^4 - \left(\frac{4}{3} - 2v_c\right)m^6 - \frac{1 + v_s}{1 + v_c} \frac{E_c}{E_s} \left(\frac{4}{3} - 2v_s\right) (1 - m^2)^3 \\
 C_{22} = \left(1 - \frac{2}{3}v_c\right) - (3 - 2v_c)m^2 + (3 - 2v_c)m^4 + \left(\frac{5}{3} - 2v_c\right)m^6 + \frac{1 + v_s}{1 + v_c} \frac{E_c}{E_s} \left(\frac{5}{3} - 2v_c\right) (1 - m^2)^3 \\
 R = -\frac{4(1 - v_s^2)}{1 + v_c} \frac{E_c}{E_s} (1 - m^2)^3 s
 \end{cases} \tag{23}$$

Once the stress states at various locations in the regional formation are obtained, the casing stress at different well depths can be calculated using the aforementioned theories, ultimately resulting in the stress distribution along the entire well section. However, the wellbore trajectory in the actual formation is not a straight line; it changes with well inclination and azimuth. To obtain the complete stress distribution along the entire casing section, multiple cross-sectional calculations and interpolation are needed. Analytical calculations are theoretically feasible but impractical in practice. Therefore, it is necessary to use finite element calculation tools to closely approximate the reservoir's geological structure, stress distribution, spatiotemporal evolution of the fracturing modification area, and wellbore trajectory. This approach allows for calculating the casing stress distribution in multiple horizontal wells within the platform and predicting potential casing failure locations.

3. Integrated geo-engineering modeling

3.1. Construction of geomechanical finite element model

To calculate and analyze the interference of horizontal well fracturing on the stress field around neighboring wells and casing deformation failure under the 'well factory' model, it is crucial to obtain the regional and wellbore stress distribution. From the previous theoretical analysis, it can be understood that the stress distribution state of the regional reservoir is controlled by geological factors such as original geological features and rock mechanical properties, as well as by engineering factors like the modified fracture network area formed by fracturing operations. Therefore,

we used an integrated geological-engineering approach by establishing a seepage-mechanics coupled geomechanical finite element model that retains the original geological features of the reservoir. After calculating the original stress distribution state of the reservoir, we continued to obtain the disturbance to the regional stress field caused by fracturing operations. In this integrated model, we embedded multiple well casings on the same platform based on the operational characteristics of the "well factory" model and the actual wellbore trajectory. Additionally, based on the sequence of fracturing operations, we restored the four-dimensional evolution process of the fracturing modification area in both time and space domains, simulating the impact of stress disturbances during fracturing operations on the casing stress distribution. Based on this, we predicted the risk of casing deformation and failure and proposed targeted preventive measures.

Establishing a regional reservoir geomechanical model involves utilizing existing geological models to analyze the characteristics of regional in-situ stress distribution. The selected area spans 2500 m × 2800 m, with depths ranging from 3150 to 4150 m and a total thickness of 1000 m, illustrated in Fig. 3. The geological layer interface features in this model were established using seismic profiles in geological modeling software. Then, based on the spatial coordinates of each point on the layer interface, a solid model was created using coordinate transformation and subsequently meshed. The calculated reservoir includes a total of 14 geological layers. Cap layer and base layer were added above and below the reservoir to facilitate the application of model boundary conditions. Surrounding rock areas were also added around the reservoir to eliminate boundary effects in the calculations. Faults in reservoirs have the possibility of slipping after being activated during

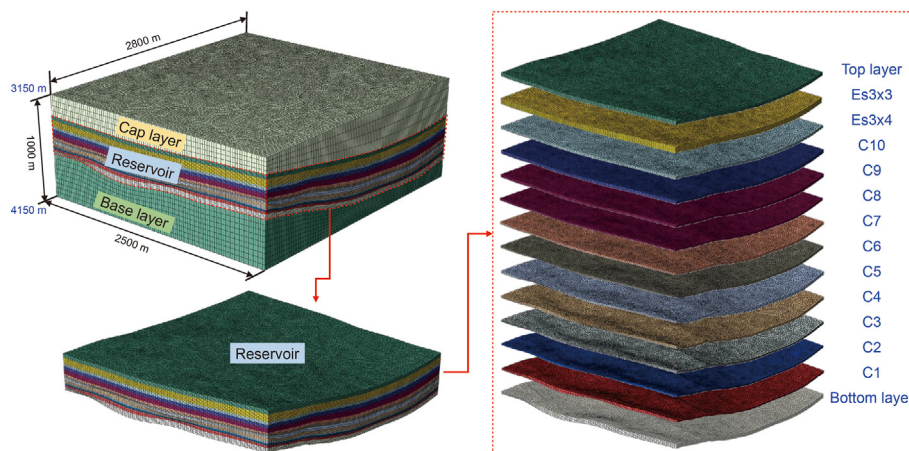


Fig. 3. Three-dimensional geomechanical finite element model of regional reservoir.

hydraulic fracturing, and geological features such as natural fractures and bedding also have a certain influence on stress distribution. However, it is difficult for us to consider the impact of fault or natural fracture activation induced by fracturing operations in this study. Because the scale of the geomechanical model we established is much larger than the scale of natural fractures in the reservoir, the actual spatial distribution state of natural fractures and their occurrence information are difficult to obtain. If we consider the random distribution of natural fractures, the accuracy of this large-scale geomechanical finite element model calculation is not enough to accurately characterize the sliding of fractures. Moreover, in the calculation of the larger-scale in-situ stress distribution, geological features such as smaller natural fractures or bedding have no obvious effect on the distribution of overall in-situ stress. Therefore, when we model the reservoir geomechanics, except for the fracture area transformed by hydraulic fracturing, we consider the rest as entities without fractures. For large-scale faults, the activation and slip of faults will indeed cause serious casing deformation and well-to-well interference. However, there is no large fault passing through the target area selected in this study, so it is not reflected in the model, and the impact of fault slip on casing deformation is not considered.

From the geological model, the wellbore positions and trajectories for each individual well in the region are designed and determined. A finite element model is then employed to incorporate the actual wellbore trajectories using pipe element models. Well X-1H is designed with a total depth of 5966 m and an actual vertical depth of 3679.32 m, while well X-2H has a total depth of 5911 m and a vertical depth of 3433.05 m. Both X-1H and X-2H wells utilize API standard specifications for the horizontal section casing, specifically P110 casing with a diameter of 139.7 mm and a wall thickness of 10.54 mm, featuring a minimum yield strength of 756.2 MPa. Calculating the original in-situ stress in the region involves using stress profiles from multiple individual wells as fundamental constraints. This process includes iterative batch calculations to ensure alignment between the three-dimensional in-situ stress magnitudes of each well trajectory and the logging interpretation stress profiles, determining boundary loads for the

computational model, and obtaining an accurate distribution of the three-dimensional in-situ stress field. Thus, selecting node paths corresponding to the wellbore trajectories of reference wells is essential. This process facilitates subsequent comparison of computed results with field logging interpretations of in-situ stress data from individual wells, thereby validating simulation accuracy.

The main objective of developing a geomechanical finite element model is to accurately capture the spatial distribution characteristics of regional in-situ stress. In the aforementioned model, the selected reservoir area consists of 14 minor layers, leading to significant variations in rock mechanical properties along the depth direction. Logging data provides continuous and economically viable means to obtain rock mechanical parameters continuously. Fig. 4(a) illustrates logging interpretation profiles of rock elastic modulus, Poisson's ratio, and original in-situ stress parameters for a specific exploration well within the target computation area. The logging interpretation data used here are data curves obtained by converting dynamic data measured by the acoustic time difference method into static data measured by the multi-depth core triaxial compression experiment (Hui et al., 2023). In this paper, we establish a geomechanical model based on data logging interpretation parameters as the basis for setting boundary conditions, and then through iterative calculation and boundary condition parameters modification, constantly make the calculation results in the model and multi-well logging data at the same time, so as to obtain the distribution of ground stress in three-dimensional space. This is because the logging interpretation profiles from individual wells offer only two-dimensional data along the exploration wellbore trajectory, which insufficiently represents the rock mechanical and in-situ stress parameter characteristics in three-dimensional reservoir space. Therefore, it is essential to use multiple exploration wells in the region as reference points, utilizing their logging data to establish model material parameters and boundary conditions. Simultaneously, extract the node paths in the model where the wellbore trajectories of reference wells are located, facilitating subsequent data comparisons. Then, use the finite element model for batch calculations, aiming to achieve computed results that align with logging interpretation data from

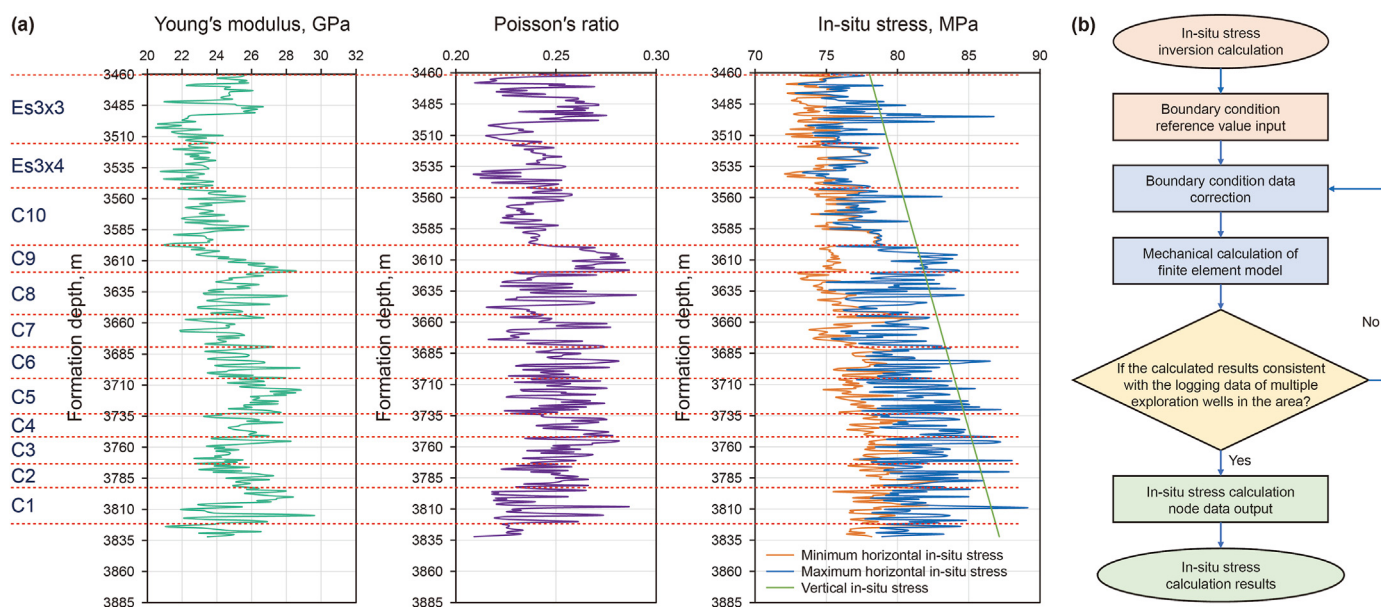


Fig. 4. Iterative method of boundary conditions for in-situ stress calculation. (a) Logging interpretation profiles of Young's modulus, Poisson's ratio, and in-situ stress magnitudes for a specific exploration well within the target area. (b) The iterative calculation procedure.

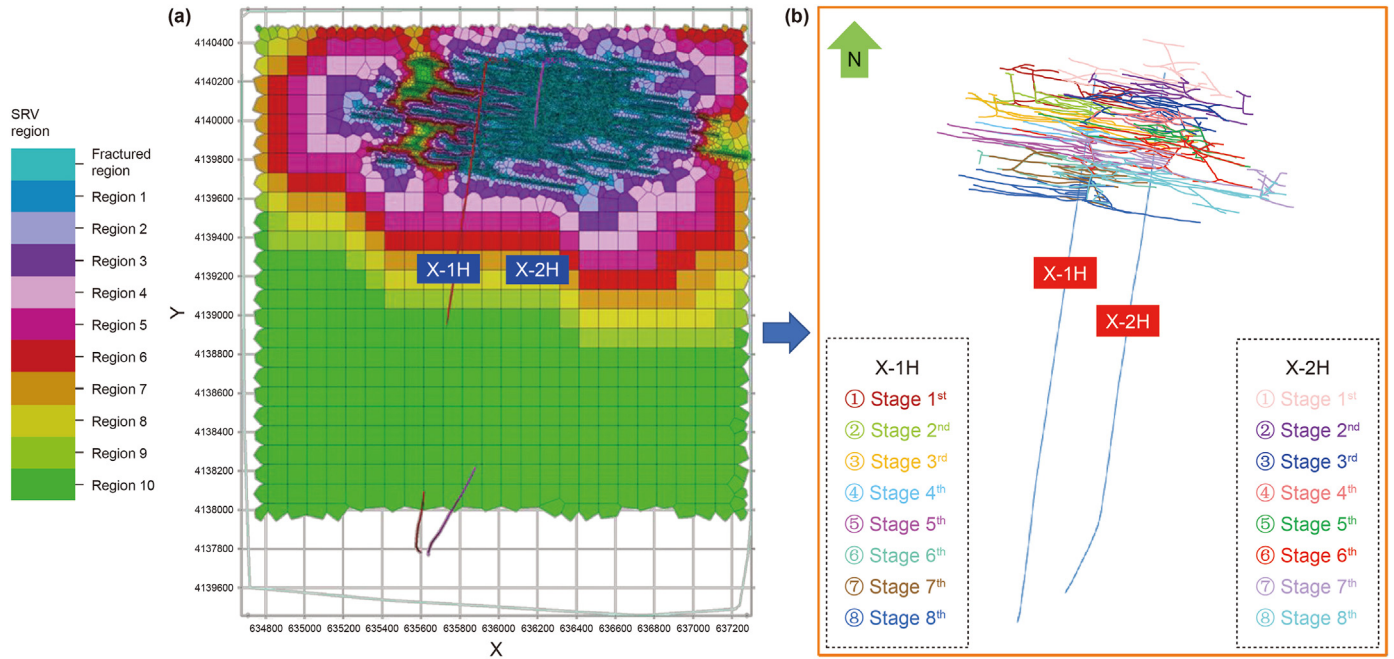


Fig. 5. Depiction of the spatiotemporal evolution process of the fracturing areas in two horizontal wells on the platform. (a) Overall rehabilitation area formed by the fracturing. (b) Spatial and temporal distribution of the main fractures from the fracturing in the two wells.

multiple individual wells as targets. This involves iterative calculations and dynamic adjustment of model material properties and boundary conditions. Retrieve data values from the designated node paths in the model during the calculation process. The calculation concludes when the computed data closely aligns with the logging interpretation data from multiple reference wells, ensuring the spatial distribution of in-situ stress in the modeled region is accurately represented. The iterative calculation procedure is shown in Fig. 4(b).

3.2. Characterization of the spatiotemporal evolution process of multi-stage fracturing

The horizontal wells in the “well factory” model use the multi-stage fracturing operations, causing the fracturing area to continuously evolve in space over time. According to the theory of rock mechanical strength degradation in fractured areas, this process continuously modifies the rock mechanical parameters of the fracturing zone, resulting in spatiotemporal changes in the stress

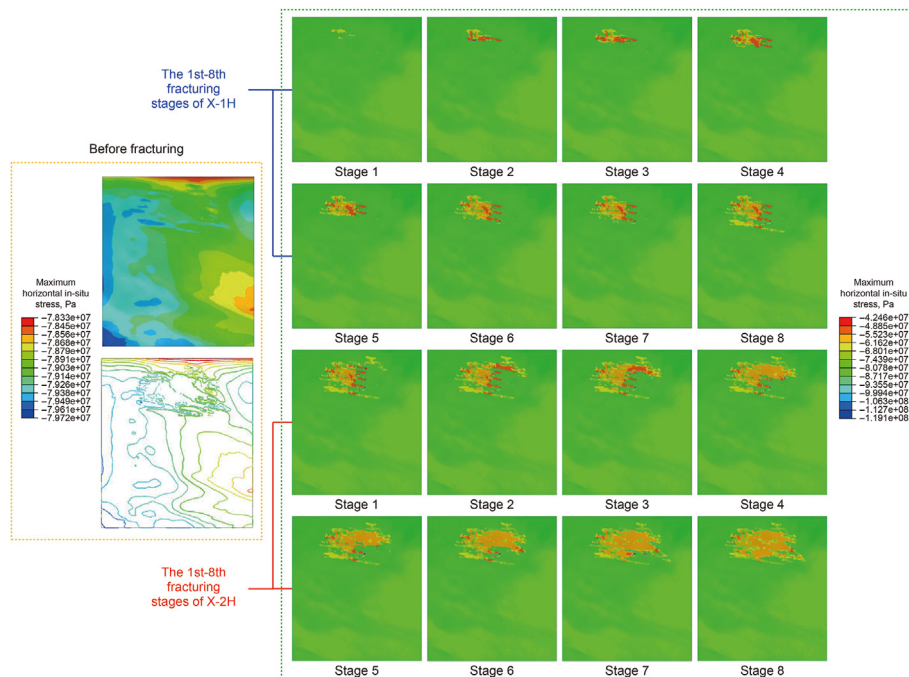


Fig. 6. Contour map of maximum horizontal stress distribution at the upper boundary of the C6 formation, and contour maps of stress distribution after operations in different fracturing stages.

field around the wellbore. Changes in the stress field around the wellbore alter the loads acting on the outer casing wall, thereby increasing the risk of casing failure.

Therefore, leveraging image recognition and mesh node coordinate identification technology, we characterized the primary fractures formed by multi-stage fracturing in two wells using the finite element model. This representation details the spatial locations and chronological appearance of the horizontal well fracturing zone on the platform, depicted in Fig. 5(a). Specifically, stages 1–8 of fracturing were conducted for wells X-1H and X-2H, with operations sequenced as fracturing X-1H first followed by X-2H, delineating the comprehensive fracturing rehabilitation area shown in Fig. 5(b).

4. Results and discussion

Before researching casing failure risks during multi-stage fracturing operations in horizontal wells on the platform, accurately calculating and characterizing the original stress field status in the region is essential. Using the geomechanical model we have established, we can obtain the distribution status of the original stress in the regional reservoir through multiple iterative simulations that match logging data from multiple exploration wells. Subsequently, it is possible to simulate the spatiotemporal evolution process of the fracturing zones in 16 segments of two horizontal wells on the platform, calculating the dynamic evolution of the regional stress field over time and space during segmented fracturing operations. Fig. 5 presents a plan view of the contour map depicting the upper boundary stress distribution in the C6 formation, where the horizontal sections of wells X-1H and X-2H are situated. Negative values in the contour map represent compressive stress.

Fig. 6 illustrates that under the original stress conditions, the maximum horizontal stress in the C6 formation ranges from 78.33 to 79.72 MPa. The maximum horizontal stress exhibits a decreasing trend from south to north, with minimal variations within the same layer due to geological characteristics. During fracturing operations, high-pressure pumps inject fracturing fluid into the formation via the wellbore, causing the formation rock to fracture due to overpressure and resulting in the formation of cracks. This process fractures the intact rock mass, leading to degradation of its mechanical properties at a macroscopic level. As fracturing fluid enters the formation along the wellbore, the increased pore pressure within the fracturing area interacts with the original stress field, leading to significant changes in both the magnitude and direction of the stress field across the model area, notably increasing non-uniformity. The high pressures from fracturing operations initiate fracturing of the formation, temporarily alleviating the stress field in the fracturing area. In the complex mechanical environment, the fractured formation may exhibit stress-depleted zones. Compared with the spatial positions of fractures shown in Fig. 5, this area corresponds to the fragmented reservoir area resulting from volumetric fracturing. However, these stress-depleted zones also generate lateral shear forces on casing and formation rocks to varying extents, resulting in radial or axial deformation along the casing. It is important to note that these stress-depleted zones are temporary regions that appear during volumetric fracturing operations. After completing volumetric fracturing operations, these regions gradually diminish over time and return to the original stress field state. However, the damage caused to the casing during fracturing operations is irreversible.

Degradation of rock mechanical properties disturbs local stress fields around the well due to hydraulic fracturing, resulting in stress redistribution. In this study, wells X-1H and X-2H underwent hydraulic fracturing operations from stage 1 to stage 8. As shown in

Fig. 6, the hydraulic fracturing zone advances over time and continuously expands in space. Within the fractured area, noticeable declines in stress levels occur due to the deterioration of rock mechanical properties. Subsequent hydraulic fracturing operations result in overlapping coverage of multiple fracturing stages, resulting in the formation of overlapping fracturing zones. In these overlapping zones, repeated fracturing leads to further deterioration in rock mechanical properties and secondary redistribution of stress. In the hydraulic fracturing zone, the maximum horizontal in-situ stress ranges from 42.46 to 55.23 MPa. In localized areas, changes in in-situ stress result in stress concentration phenomena, with in-situ stress levels possibly increasing to a maximum of 119.10 MPa. With the progression of multi-stage hydraulic fracturing, a non-uniform distribution of stress disturbance areas forms within the region. This series of stress redistribution phenomena greatly enhances the non-uniform distribution of reservoir stress, significantly increasing the non-uniformity of external loads on casing and the risk of casing deformation failure. This figure illustrates the stress distribution patterns resulting from multi-stage hydraulic fracturing. The highlighted areas indicate regions of high stress, which correlate with potential casing deformation. Understanding these stress variations is crucial for assessing the risks associated with casing failure, particularly during fracturing operations. The stress distribution not only reflects the immediate effects of hydraulic fracturing but also suggests how these changes might influence subsequent operations and well integrity.

In the hydraulic fracturing zone, the redistribution of in-situ stress results in both differences in stress magnitude and simultaneous changes in the direction of in-situ stress. Fig. 7 illustrates the vector distribution of maximum and minimum horizontal in-situ stress directions in layer C6. The study aimed to determine that the original minimum horizontal in-situ stress direction in the target area generally trends north-south, whereas the maximum horizontal in-situ stress direction trends east-west. However, as indicated by the calculation results in Fig. 6, after hydraulic fracturing, the direction of in-situ stress in the fracturing zone has become highly complex and intricate. The change in in-situ stress direction increases the uncertainty of external loads on the casing, while the complex distribution of in-situ stress directions in the hydraulic fracturing zone enhances the casing's exposure to both axial and radial shear forces.

The trajectories of the well casings for two horizontal wells on the platform have been incorporated into the geomechanics finite element model using pipe units. Consequently, the model calculates the stress distribution states on the well casing during the coupled deformation process with ongoing hydraulic fracturing, affecting the in-situ stress. The research focuses on hydraulic fracturing segment areas selected below 5000 m depth for both wells. Thus, distribution curves of the Mises stress on the casings of wells X-1H and X-2H below 5000 m depth after various hydraulic fracturing operations were extracted, as depicted in Figs. 8 and 9.

According to Fig. 8, prior to the start of hydraulic fracturing operations, the Mises stress level on the casing under the original in-situ stress was relatively low, approximately 310 MPa, well below the minimum yield strength of P110 casing, which is 756 MPa. Thus, before initiating any hydraulic fracturing operations in this platform area, the casing faced no risk of deformation failure. However, with the onset of hydraulic fracturing in well X-1H, the casing experienced escalating Mises stresses due to the intricate variations in in-situ stress across the region. Moreover, the presence of overlapping fracturing zones causes multiple intricate temporal and spatial redistributions of in-situ stress, resulting in fluctuations in Mises stress on the casing that may exceed those from the total 8 stages of hydraulic fracturing in the well. Significant Mises stress fluctuations were already evident in the casing of

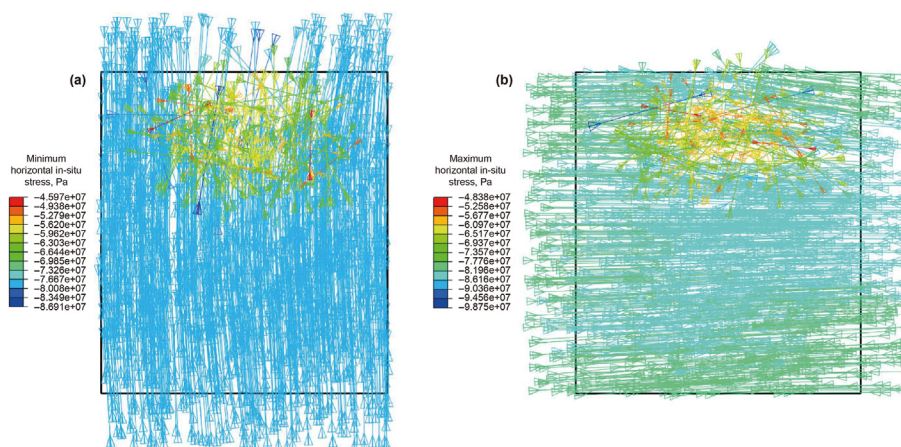


Fig. 7. Vector distribution of horizontal in-situ stress directions in the target calculation area. (a) Minimum horizontal in-situ stress. (b) Maximum horizontal in-situ stress.

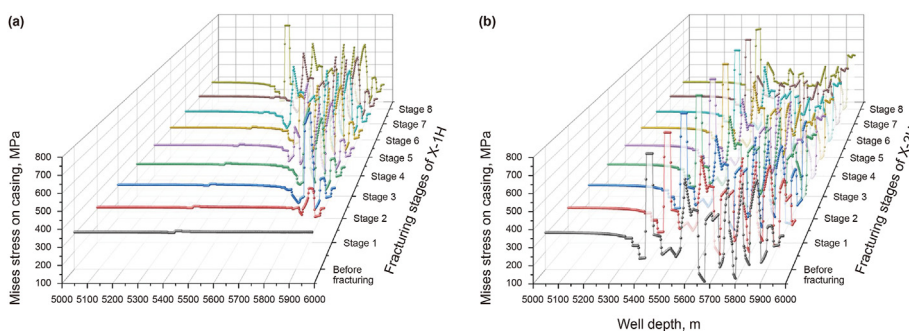


Fig. 8. Distribution curves of Mises stress on the casing of well X-1H after different fracturing stages. (a) Fracturing in well X-1H. (b) Fracturing in well X-2H.

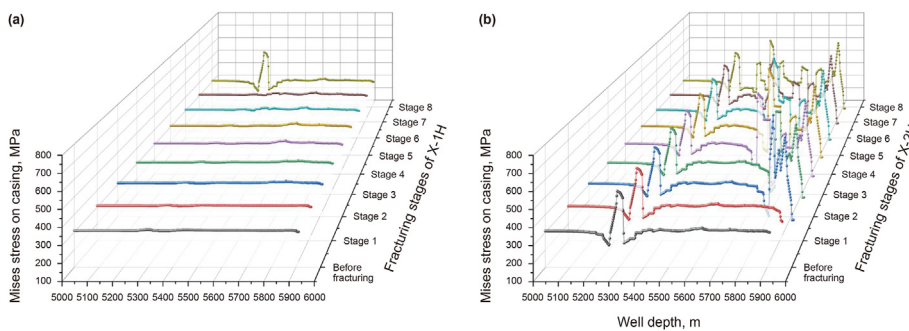


Fig. 9. Distribution curves of Mises stress on the casing of well X-2H after different fracturing stages. (a) Fracturing in well X-1H. (b) Fracturing in well X-2H.

well X-1H before commencing hydraulic fracturing operations in well X-2H. Furthermore, certain fracturing zones in well X-2H overlapped with those previously completed in well X-1H, resulting in additional changes in rock mechanical properties and pore pressure in the overlapping area. This increased the complexity of the wellbore mechanical environment and intensified the rise in Mises stress on the casing. For instance, the Mises stress at the bottom of well X-1H continued to rise during the hydraulic fracturing process in well X-2H, thereby heightening the risk of deformation failure.

Similarly, Mises stress data from the casing below 5000 m depth in well X-2H was extracted using the same approach. Fig. 9 depicts the distribution curve of Mises stress on the casing of well X-2H following various fracturing stages. The initial 7 stages of fracturing

in well X-1H had a relatively minor effect on the Mises stress of the casing in well X-2H. However, fractures generated during the 8th stage of fracturing in well X-1H extended into the spatial region where the casing of well X-2H is situated. Consequently, following the 8th stage of fracturing, the casing stress in well X-2H was notably affected by the nearby well's fracturing operations, leading to an increase in Mises stress on the casing in the corresponding segment. Following the initiation of hydraulic fracturing in well X-2H, subsequent sections of casing began to show stage-by-stage fluctuations in Mises stress, with the frequency of fluctuations far surpassing the number of fracturing stages in this well.

Based on the distribution of Mises stresses on the casings of both wells, it can be concluded that the primary mechanism causing casing deformation during hydraulic fracturing operations is the

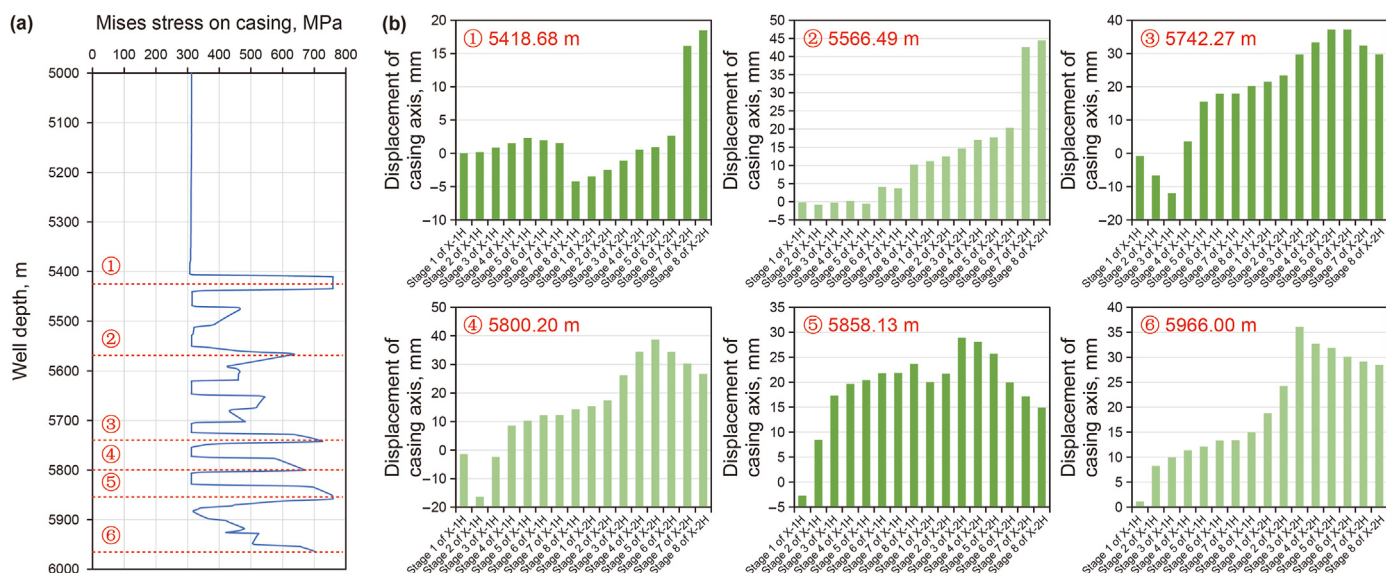


Fig. 10. Prediction of high-risk points for casing damage and analysis of casing deformation in the X-1H well. (a) Mises stress distribution curve after fracturing and calibration of high-risk points for casing deformation. (b) Displacement at high-risk prediction points for casing damage in different fracturing stages.

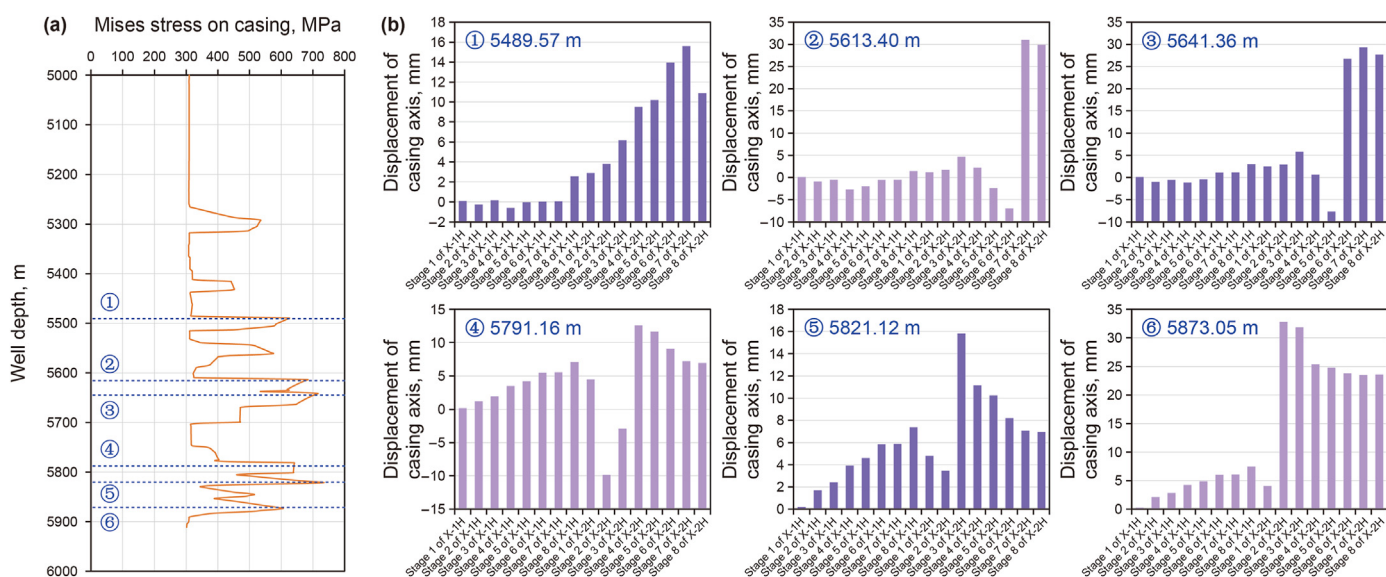


Fig. 11. Prediction of high-risk points for casing damage and analysis of casing deformation in the X-2H well. (a) Mises stress distribution curve after fracturing and calibration of high-risk points for casing deformation. (b) Displacement at high-risk prediction points for casing damage in different fracturing stages.

repeated and complex redistribution of the regional stress field. The overlapping of fracturing zones within different stages of the same well, as well as between neighboring wells on the platform, directly leads to multiple redistributions of the stress field around the well. The increasing non-uniformity of the stress field subjects the casing to varying external loads continuously, resulting in elevated Mises stresses and significantly increased risks of casing deformation failure.

To accurately predict the risk of casing failure, we extracted the Mises stress distribution curves of the casings from two wells after completing the entire fracturing process. Six high-stress locations were identified as high-risk prediction points for casing failure, as depicted in Figs. 10(a) and 11(a). On the casing of well X-1H, among these high-risk points, Mises stresses exceed 700 MPa at four locations, surpassing the minimum yield strength of P110 casing

material. These locations are susceptible to deformation failure during subsequent long-term service due to mechanical effects such as cyclic pressure loading from fracturing, reservoir depletion after extended production, and rock creep in the formation. Figs. 10(b) and 11(b) analyze the displacement of these high-risk points for casing failure in each well at different fracturing stages, aiming to understand the timing and variation of casing deformation. Fig. 10(b) illustrates that casing deformation initially occurs at a depth of 5966.00 m in well X-1H, with a displacement of 8.25 mm along the casing axis after the second fracturing stage. Subsequent fracturing operations lead to gradual accumulation of casing deformation, but a significant increase occurs after the start of fracturing in well X-2H, reaching 36.08 mm after the fourth fracturing stage in X-2H. Similar analysis applies to other high-risk prediction points for casing failure in well X-1H. These points on

the casing begin to exhibit varying degrees of deformation during the fracturing process in well X-1H, with notable increases during subsequent fracturing operations in well X-2H. Some time points show negative displacement of the casing, indicating that the complex redistribution of the stress field around the well, caused by fracturing, subjects the casing to forces in different directions at different times, resulting in displacements in various directions. These figures identify the high-risk zones for casing deformation based on stress distribution data. The regions marked as high risk are analyzed in relation to well spacing and fracturing techniques. These insights are essential for field engineers as they provide actionable information for optimizing well design and spacing strategies to mitigate casing failure. By understanding the relationship between the identified risk zones and operational parameters, operators can make informed decisions to enhance well integrity and performance.

Fig. 11 presents the analysis data on high-risk prediction points for casing damage and deformation in well X-2H. Well X-2H identifies 6 high-risk points for casing failure, with only 2 points exceeding 700 MPa in Mises stress, compared to well X-1H. Fig. 11(b) illustrates that during the fracturing stage of well X-2H, the displacement of the casing axis is relatively minor, influenced primarily by its specific fracturing operations. For instance, at a depth of 5873.05 m in well X-2H, after the second fracturing stage, the casing axis displacement sharply increases from 4.04 to 32.76 mm, resulting in significant S-shaped deformation over a short period, thereby escalating the risk of failure. Comprehensive analysis indicates that overlapping fracturing areas between different stages within the same well can gradually increase casing axis displacement or even cause its reversal. This overlap, caused by neighboring well operations, is the primary reason for the sharp increase in casing axis displacement.

In summary, hydraulic fracturing operations induce stress deficits within the fracturing area, accompanied by significant variations in the regional stress field. These multiple changes exacerbate the non-uniformity of external loads on the casing, leading to substantial stress fluctuations at corresponding casing positions. Local segments of the wellbore casing experience Mises stress that approaches or exceeds the material's minimum yield strength, posing a high risk of failure. Analysis of casing axial displacement at high-risk prediction points reveals that mutual overlap between fracturing areas from different stages is the primary factor contributing to increased casing deformation. Following hydraulic fracturing, fractures extending from horizontal wells within the platform to adjacent wellbore areas result in a sharp increase in axial displacement of the adjacent well casing. Therefore, to mitigate casing deformation failure at high-risk prediction points, we propose the following measures: firstly, enhancing the casing material grade in the targeted reservoir region to increase its minimum yield strength; secondly, optimizing spatial distribution resulting from hydraulic fracturing to mitigate complex stress redistribution around the wellbore; and thirdly, during well trajectory design, focusing on designing hydraulic fracturing transformation areas and ensuring adequate well spacing to prevent interference between adjacent horizontal wells on the platform due to overlapping fracturing areas. In the analysis of well spacing optimization, we recognize its crucial role in mitigating casing failure. Based on our model results, we recommend specific well spacing distances that can significantly reduce the risk of casing deformation. Based on the specific geological characteristics and rock mechanics characteristics, it is necessary to simulate the fracture shape of multistage hydraulic fracturing first to obtain the limit value of hydraulic fracture extension length, and the well spacing of well layout design should be slightly higher than the fracture extension length. These distances are derived from our

stress distribution analysis, which indicates that maintaining this spacing can effectively minimize stress concentration in adjacent wells.

At present, there are still many theoretical assumptions in this model, so here we make some prospects for future research:

Future research directions: We will suggest conducting further field studies to validate the geomechanical model across various geological environments to ensure its applicability.

Geological variability: We will discuss the need to investigate how different geological characteristics, such as faulting and natural fractures, may influence casing integrity and the effectiveness of our mitigation strategies.

Applications in diverse settings: We will highlight how the insights from our study can be applied to optimize drilling operations and casing design in other unconventional reservoirs, addressing specific geological challenges.

5. Conclusion

This paper conducts an in-depth study on the interference of multi-stage hydraulic fracturing operations on neighboring well casings' deformation and failure in the "well factory" model. The research results show that hydraulic fracturing operations on multi-well platforms have significant impacts on inter-well interference, causing neighboring well casings to experience complex non-uniform external loads, increasing the risk of casing deformation and failure. The specific conclusions are as follows:

- (1) Stress field redistribution in fracturing areas: In the "well factory" model, hydraulic fracturing operations on multi-well platforms cause degradation of the reservoir rock's mechanical properties, disturb and redistribute the original stress field, applying additional shear stress to neighboring well casings. This enhances the non-uniformity of the external loads on the casings, leading to deformation or even failure.
- (2) Intensified inter-well interference: The overlapping fracturing zones of multiple wells on the platform cause mutual interference between the fracturing operations of adjacent wells. Inter-well interference leads to multiple redistributions of the regional stress field, significantly increasing the complexity and uncertainty of the external loads on neighboring well casings, further raising the risk of casing deformation and failure.
- (3) Interference between sections within the same well: Additionally, the modified areas formed by different fracturing sections within the same well can overlap, exacerbating the non-uniformity of the axial load on the casing to a certain extent, increasing the risk of S-shaped deformation or even failure.
- (4) High-risk point identification: By analyzing the Mises stress distribution of the casing during fracturing, multiple high-stress locations caused by inter-well interference were identified. The stress values at these high-stress locations are close to or exceed the yield strength of the casing material, making them prone to deformation and failure due to mechanical effects during subsequent long-term service.
- (5) Measures to mitigate inter-well interference: To reduce the risk of casing deformation and failure caused by inter-well interference in the "well factory" model, it is recommended to upgrade the casing material grade in the target reservoir area to increase its yield strength. However, to fundamentally resolve the issue of casing deformation and failure, optimizing the spatial distribution of inter-well hydraulic fracturing to reduce complex stress redistribution and

reasonably arranging well spacing in well trajectory design to avoid interference caused by overlapping fracturing zones between neighboring wells are crucial.

- (6) To mitigate casing failure, we suggest several practical applications of our findings: Operators can adjust well spacing based on identified stress shadow zones to minimize interference and reduce the risk of casing deformation. Choosing casing materials with higher strength properties can help withstand increased stresses observed in high-risk areas, enhancing well integrity. Implementing real-time monitoring systems allows operators to track stress variations during operations, enabling proactive management of well integrity.

In summary, this study uses a geology-engineering integrated model, combined with stress field evolution simulation and multi-stage fracturing stress variation analysis, to focus on the interference of hydraulic fracturing in the “well factory” model on neighboring well casings. It proposes new perspectives and methods for predicting casing failure risk, providing important references for assessing casing integrity in complex stress environments. In practical applications, the model can be established and adjusted based on the actual geological conditions of the target area. During drilling and fracturing design, the model can be used to predict casing deformation in the “well factory” model, which can then be used to optimize drilling and fracturing design. The proposed research methods and calculation processes can be applied to analyze any relatively tight unconventional oil and gas wells. Due to limitations in computational power, our current model does not fully consider the possibility of fault activation and slip in the reservoir, nor does it consider the impact of geological features such as natural fractures and bedding on stress distribution. In the future, we will gradually add various geological and engineering factors that need to be considered to this model, making the model's calculation results more accurate and reliable.

CRediT authorship contribution statement

Yu-Heng Tuo: Writing – original draft, Visualization, Investigation, Formal analysis, Data curation, Conceptualization. **Tie-Jun Lin:** Validation, Resources, Project administration, Funding acquisition. **Hao Yu:** Visualization, Validation, Project administration, Methodology, Funding acquisition, Conceptualization. **Zhang-Hua Lian:** Supervision, Software, Resources, Project administration. **Fang-Xin Chen:** Writing – review & editing, Visualization.

Data availability statement

All data that support the findings of this study are included in this manuscript and its supplementary information files.

Financial Support

This work was supported by the National Natural Science Foundation of China (No. 52104008 & No. 52274042) and the Natural Science Foundation of Sichuan, China (No. 2024NSFSC0963).

Declaration of competing interest

The authors declare that they have no known competing financial interests or personal relationships that could have appeared to influence the work reported in this paper.

Acknowledgements

The authors are grateful to the support from the National Natural Science Foundation of China (No. 52104008 & No. 52274042) and the Natural Science Foundation of Sichuan, China (No. 2024NSFSC0963).

References

- Dong, K., Liu, N., Chen, Z., et al., 2019. Geomechanical analysis on casing deformation in Longmaxi shale formation. *J. Petrol. Sci. Eng.* 177, 724–733. <https://doi.org/10.1016/j.petrol.2019.02.068>.
- Forbes, B., Ehler, J., Wilczynski, H., 2012. *The Flexible Factory: the Next Step in Unconventional Gas Development*. Schlumberger Business Consulting.
- Guo, X., Jin, Y., Huang, L., et al., 2021. Research status and discussion of horizontal well interference in shale oil and gas reservoirs. *Oil Drill. Prod. Technol.* 43 (3), 348–367. <https://doi.org/10.13639/j.odpt.2021.03.013> (in Chinese).
- He, D., Wang, L., Ji, G., et al., 2012. Well spacing optimization for Sulige tight sand gas field, NW China. *Petrol. Explor. Dev.* 39 (4), 491–497. [https://doi.org/10.1016/S1876-3804\(12\)60066-4](https://doi.org/10.1016/S1876-3804(12)60066-4).
- Hui, G., Chen, Z., Ryan, S., et al., 2023. Intricate unconventional fracture networks provide fluid diffusion pathways to reactivate pre-existing faults in unconventional reservoirs. *Energy* 282, 128803. <https://doi.org/10.1016/j.energy.2023.128803>.
- Huls, B., Hurey, M., Johnson, J., 2013. Gas factory, operational efficiencies in the marcellus shale lead to exceptional results. SPE Eastern Regional Meeting, Pittsburgh, Pennsylvania, USA. SPE-165708-MS. <https://doi.org/10.2118/165708-MS>.
- Jia, Y., Wu, W., Kong, X., 2020. Injection-induced slip heterogeneity on faults in shale reservoirs. *Int. J. Rock Mech. Min. Sci.* 131, 104363. <https://doi.org/10.1016/j.ijrmms.2020.104363>.
- Kostić, S., Vasović, N., Franović, I., 2018. Effect of viscosity of fault filling on stick-slip dynamics of seismogenic fault motion: a numerical approach. In: *ISRM Eur. Rock Mech. Sympos. - EUROCK 2018*, St. Petersburg, Russia. ISRM-EUROCK-2018-069, VOLS 1 AND 2, pp. 539–544.
- Kumar, D., Ghassemi, A., 2016. A three-dimensional analysis of simultaneous and sequential fracturing of horizontal wells. *J. Petrol. Sci. Eng.* 146, 1006–1025. <https://doi.org/10.1016/j.petrol.2016.07.001>.
- Lele, S., Tyrrell, T., deMartin, B., 2020. Effect of faulting regime, Poisson's ratio, and non-uniform reservoir deformation on fault reactivation due to injection and production. 54th U.S. Rock Mechanics/Geomechanics Symposium, Physical Event Cancelled. ARMA-2020-1595.
- Li, D., He, Z., Wang, R., et al., 2023. Research on the effect of shale core mechanical behavior on casing deformation. *Processes* 11 (1), 274. <https://doi.org/10.3390/pr11010274>.
- Lian, Z., Yu, H., Lin, T., et al., 2015. A study on casing deformation failure during multi-stage hydraulic fracturing for the stimulated reservoir volume of horizontal shale wells. *J. Nat. Gas Sci. Eng.* 23, 538–546. <https://doi.org/10.1016/j.jngse.2015.02.028>.
- Liu, Y., Chen, P., Ma, T., et al., 2017. Application of well factory drilling technology in shale gas development in the Sichuan basin. SPE/IATMI Asia Pacific Oil & Gas Conference and Exhibition, Jakarta, Indonesia. SPE-186914-MS. <https://doi.org/10.2118/186914-MS>.
- Lu, Q., Liu, Z., Guo, J., et al., 2021. Hydraulic fracturing induced casing shear deformation and a prediction model of casing deformation. *Petrol. Explor. Dev.* 48 (2), 460–468. [https://doi.org/10.1016/S18763804\(21\)60037-X](https://doi.org/10.1016/S18763804(21)60037-X).
- Nandlal, K., Weijermars, R., 2022. Shale well factory model reviewed: Eagle Ford case study. *J. Pet. Sci. Eng.* 212 (Suppl C), 110158. <https://doi.org/10.1016/j.petrol.2022.110158>.
- Rexilius, J., 2015. The well factory approach to developing unconventional: a case study from the Permian Basin wolfcamp play. SPE/CSUR Unconventional Resources Conference, Calgary, Alberta, Canada. SPE-175916-MS. <https://doi.org/10.2118/175916-MS>.
- Roussel, N., Sharma, M., 2011. Strategies to minimize frac spacing and stimulate natural fractures in horizontal completions. SPE Annual Technical Conference and Exhibition, Denver, Colorado, USA. SPE-146104-MS. <https://doi.org/10.2118/146104-MS>.
- Tuo, Y., Yu, H., Lian, Z., et al., 2024. Impact of fault slip induced by water injection on casing deformation: a numerical study. *Petrol. Sci. Technol.* 1–24. <https://doi.org/10.1080/10916466.2024.2356734>.
- Wang, H., Mao, L., Zhu, J., et al., 2024. Adjacent well casing damage caused by fluid pressure intrusion in multistage fracturing. *Petrol. Sci. Technol.* 1–21. <https://doi.org/10.1080/10916466.2024.2347958>.
- Wang, Y., Li, X., Wang, J., et al., 2015. Numerical modeling of stress shadow effect on hydraulic fracturing. *Nat. Gas Geosci.* 26 (10), 1941–1950. <https://doi.org/10.11764/j.issn.1672-1926.2015.10.1941> (in Chinese).
- Warpinski, N., Mayerhofer, M., Vincent, M., et al., 2009. Stimulating unconventional reservoirs: maximizing network growth while optimizing fracture conductivity. *J. Can. Petrol. Technol.* 48 (10), 39–51. <https://doi.org/10.2118/114173-PA>.
- Xi, Y., Li, J., Fan, L., et al., 2021. Mechanism and numerical simulation of a new device of bypass cementing device for controlling casing shear deformation induced by fault slipping. *J. Petrol. Sci. Eng.* 196, 107820. <https://doi.org/10.1016/j.petrol.2021.107820>.

- [j.petrol.2020.107820](https://doi.org/10.1016/j.petrol.2020.107820).
- Yin, F., Xiao, Y., Han, L., et al., 2018. Quantifying the induced fracture slip and casing deformation in hydraulically fracturing shale gas wells. *J. Nat. Gas Sci. Eng.* 60, 103–111. <https://doi.org/10.1016/j.jngse.2018.10.005>.
- Yu, H., Dahi Taleghani, A., Lian, Z., et al., 2019. Impact of asymmetric stimulated rock volume on casing deformation in multi-stage fracturing; A case study. SPE Annual Technical Conference and Exhibition, Calgary, Alberta, Canada. SPE-195944-MS. <https://doi.org/10.2118/195944-MS>.
- Yu, H., Dahi Taleghani, A., Lian, Z., et al., 2020. On how asymmetric stimulated rock volume in shales may impact casing integrity. *Energy Sci. Eng.* 8 (5), 1524–1540. <https://doi.org/10.1002/ese3.610>.
- Yu, H., Tuo, Y., Lin, T., et al., 2023. On how water injection may induce fault reactivation and slippage: a numerical method. *Petroleum* 10 (4), 646–659. <https://doi.org/10.1016/j.petlm.2023.07.003>.
- Yu, Y., Zhu, W., Li, L., et al., 2017. Analysis on stress shadow of mutual interference of fractures in hydraulic fracturing engineering. *Chin. J. Rock Mech. Eng.* 36 (12), 2926–2939. <https://doi.org/10.13722/j.cnki.jrme.2017.0405> (in Chinese).